



# Heat transfer and thermal–hydraulic evaluations of cross-circular grooved rectangular flow ducts depending on rectangular baffle design parameters

Koray Karabulut<sup>a</sup>

Electric and Energy Department, Sivas Technical Sciences Vocational School, Sivas Cumhuriyet University, 58140 Sivas, Turkey

Received: 20 October 2023 / Accepted: 13 February 2024  
© The Author(s) 2024

**Abstract** The cross-grooved rectangular flow ducts are largely used for plate heat exchangers. In this work, so as to better the heat transfer in cross-grooved rectangular ducts with circular grooves, rectangular baffles were located in the flow duct, and the influences of the rectangular baffle angles and heights on the features of heat transfer were numerically performed in detail. Equations of Navier–Stokes and energy were resolved by employing a program of Ansys-Fluent with  $k$ – $\epsilon$  turbulence model as steady and three-dimensional. Air employed as working fluid has a temperature of inlet 293 K while the circular groove's wall temperature is 373 K. Rectangular baffles have various angles of 30°, 60°, and 90°, and heights of 0.25  $H$ , 0.5  $H$ , and 0.75  $H$ . The mean Nusselt number ( $Nu_m$ ), temperature, turbulence kinetic energy (TKE), pressure, and PEC (Performance Evaluation Criterion) number of the flow duct with rectangular baffles were evaluated by comparing it with the cross-circular grooved channel non-baffle. Besides, the contours of velocity, turbulence kinetic energy, temperature, and velocity vector were exhibited for the cross-circular grooved rectangular channels with different baffle angles and height arrangements. Results were matched with experimental and numerical outcomes of the study found in the literature, and it was observed that they were fairly coherent. For  $Re = 6000$ , the number of  $Nu_m$  increases by 180.48% in the duct with a 90° angle and 0.75  $H$  baffle height compared to the duct non-baffle, and for 30° baffle angle, the PEC value at 0.25  $H$  baffle height is 66.88% higher than that in the 0.5  $H$ .

## List of symbols

$A_c$	Cross section of jet inlet, $m^2$
$H$	Duct height, m
$L$	Duct length, m
$W$	Duct width, m
$D_h$	Hydraulic diameter of the duct, m
$h$	Local convective heat transfer coefficient, $Wm^{-2}K^{-1}$
$k$	Thermal conductivity, $Wm^{-1}K^{-1}$
$V$	Velocity of the fluid in the duct entry, $ms^{-1}$
$c_p$	Fluid specific heat capacity, $Jkg^{-1}K^{-1}$
$P$	Perimeter length of jet inlet cross section, m
$p$	Pressure, $Nm^{-2}$
$T$	Temperature, K
$u, v, w$	Components of velocity in x,y,z directions, $ms^{-1}$
$u', v', w'$	Components of fluctuating velocity in x,y,z directions, $ms^{-1}$
$\bar{u}, \bar{v}, \bar{w}$	Velocities of mean in coordinates, $ms^{-1}$
Re	Reynolds number ( $= V_\infty D_h / \nu$ ), dimensionless
Nu	Local Nusselt number ( $= h L / k$ ), dimensionless

## Greek symbols

$\mu$	Viscosity of dynamic, $kg s^{-1} m^{-1}$
$\mu_t$	Viscosity of turbulence, $kg s^{-1} m^{-1}$

<sup>a</sup> e-mails: [kkarabulut@cumhuriyet.edu.tr](mailto:kkarabulut@cumhuriyet.edu.tr); [koray.karabulut@hotmail.com](mailto:koray.karabulut@hotmail.com) (corresponding author)

$\nu$	Viscosity of kinematic, $\text{m}^2\text{s}^{-1}$
$\rho$	Density, $\text{kgm}^{-3}$
$\phi$	Term of viscous dissipation, $\text{m}^2\text{s}^{-3}$
$k'$	Kinetic energy of turbulence, $\text{m}^2\text{s}^{-2}$
$\varepsilon$	Dissipation rate of turbulence, $\text{m}^2\text{s}^{-3}$
$\varphi$	Rectangular baffle angle, ( $^\circ$ )

## Subscripts

s	Surface
sm	Surface mean
$\infty$	Fluid
m	Mean

## 1 Introduction

In late years, the enhancement in energy use and the necessity of using energy-efficient and economical devices have revealed the necessity of developing heat exchangers in this direction. In line with the demand for heat exchangers that are economical, high-performance, lightweight and space-saving, the interest in researching compact surfaces is increasing. Compact heat exchangers, defined by their surface area of high heat transfer against their volumetric rates, attract great interest due to their coefficients of high heat transfer when compared to other types of heat exchangers.

Plate heat exchangers which are compact present maximum technology, efficiency and user-friendliness in widescale implementations from particular technology to the motor vehicle industry and broad industry usages from nourishment processing to actinic and medication implementations. In the meantime, cross-grooved ducts are used in plate heat exchangers and have some advantages like the high coefficient of heat transfer and high strength of mechanical besides the disadvantage of a big drop of pressure.

In the heat exchangers of plate type, a series of cross-grooved flow ducts exist and these ducts are created by giving the shape of an angle to contiguous sheets, so, warm and cool fluids are separated from one another via these sheets. Thus, the basic geometrical characteristics are determined: inclination angle, angle of apex, height and pitch of groove of the cross-grooved duct. The groove cross section of the cross-grooved duct can create a vortex and subsidiary flow in grooves, which enhances heat transfer between contiguous flow ducts. This enhancement fundamentally belongs to duct geometric features. Therefore, designing and optimizing processes of the cross-grooved ducts are one of the most important issues on account of heat transfer and properties of flow, and related studies are carried out numerically and experimentally by researchers [1].

Feng et al. [2] researched the influences of three distinct types of trapezoidal baffles on the features of heat transfer and flow of the cross-grooved triangular flow ducts. The Nu number, f factor and the value of the PEC number were also evaluated. They achieved an increase in PEC value of up to 30% compared to without baffle. Liu and Niu [3] carried out the survey employing a computational heat transfer study for the geometrical influence on the thermohydraulic properties of a cyclical cross-grooved duct. The influence of the angle of apex and ratio of aspect on heat transmission, pressure drop, and performance of thermohydraulic in the grooved duct was researched for this aim. Their results pointed out that the angle of the apex effectively influenced the loss of pressure and heat transfer in a triangular grooved duct. With the aim of improvement of heat transfer, cross-grooved triangular ducts at the apex angles of  $90^\circ$  and  $120^\circ$  were advised. Besides, it was determined that the rate of aspect has a comparatively strong effect on frictional loss in comparison to its influence on the heat transfer for the performed situations. Chen et al. [4] compared four triangular grooved ducts. According to the results obtained, the triangular grooved ducts have the most appropriate increase effect in terms of gradients of velocity, temperature and pressure. Chen [5] researched the mean values of friction factor and Nu numbers for a triangular grooved duct under the conditions of laminar flow and uniform wall temperature. It was discovered that for higher values of Re numbers, recirculation regions in the lower grooves are a predominant effect for heat transfer, while for lower values of Re numbers, parallel flows in the upper grooves are the dominant effect. In another study, the economic effect and rate of entropy generation were evaluated for a heat exchanger with triangular grooved ducts by Men et al. [6]. The duct height  $H$ , angle of apex  $\theta$ , duct number of each layer on the fresh air side  $n_f$ , and exhaust air side  $n_e$ , and the total number of plates  $n_h$  were taken into consideration as geometric design parameters. Sharif et al. [7] designed to investigate the influence of the angle of the apex on the thermal and hydraulic properties of triangular grooved heat exchangers for a range of Re numbers of 310–2064 by employing a 3D CFD approach with the Reynolds stress model. By increasing the angle of the apex both the drop of pressure and coefficient of heat transfer enhance. Focke and Knibbe [8] experimentally and numerically searched the transfer of heat in a cross-grooved duct used for compact heat exchangers. They used the angle of the groove, geometric ratio, and Re number as research parameters. They found that the mean Nu number enhances almost the ratio of  $\text{Re}^{2/3}$  for whole geometry, and investigated the change of Nu number with the angle of groove and pitch-to-height ratio. Hall et al. [9] experimentally reached a correlation of the coefficient of mass transfer for a heat exchanger with triangular grooved with an angle of apex of  $90^\circ$  for the range of Re number of 200–2300.

They discovered that the regime of the flow was not laminar in the studied Re number range. Zhang and Che [10] obtained the Nu number, Nu and friction factor,  $f$  for grooved ducts with different groove profiles of sinusoidal, triangular, rectangular, and elliptic. The results pointed out that the Nu and  $f$  of the flow duct with trapezoidal grooved profiles are higher than those of the other ducts. Liu and Niu researched the effects of the angles of the apex on the thermohydraulic properties of triangular grooved ducts. They discovered that the ducts with the angles of the apex of  $90^\circ$  and  $120^\circ$  have the highest heat transfer coefficients. Leung and Probert [11] searched the thermal features of three types of heat exchangers with isosceles triangular grooves having the angles of the apex of  $40^\circ$ ,  $60^\circ$ , and  $90^\circ$  at a Re number range of 5000–20000. Zhang [12] numerically analyzed the properties of heat transfer of a triangular grooved flow duct with a  $60^\circ$  apex angle using a turbulence model of  $k-\omega$  for the 100–6000 Re number range. In their work, they proposed two equations for the Nu number at constant boundary conditions of the flux of heat and temperature. Doo et al. [13] suggested innovator surfaces to enhance the thermal–hydraulic performance of the grooved flow ducts. The suggested surface geometries created a 15% reduction in pressure drop without causing a significant reduction in Nu number. However, many researchers studied innovative surface geometries in order to enhance the performance of heat transfer of grooved ducts [14–18]. In addition to this, the heat transfer improvements that can be achieved with passive surface shapes are limited.

Baffles, commonly employed in heat exchangers of shell-and-tube, are largely used to increase the transfer of heat area. In addition, baffles have the ability to shift the main flow direction, and enhance the mixing of the flow and transfer of heat. However, there are not many works on baffles that cause increased heat transfer by creating the flow of turbulence in the duct at low Re numbers. Li and Gao [19] researched the heat transfer of convective in a grooved flow duct with a triangular baffle by using the principle of synergy. Their results pointed out that heat transfer can be increased with a large loss of pressure. Li et al. [20] searched the angles of the apex of  $60^\circ$ ,  $90^\circ$  and  $120^\circ$  and baffle settlement on the heat and flow properties of the triangular grooved duct with trapezoidal baffles. Computational results of friction factor, Nu number, and PEC were analyzed for different duct arrangements. The outcomes illustrated that the  $f$  value for the ducts with apex angles of  $60^\circ$  and  $90^\circ$  are close to each other but higher than that of  $120^\circ$ . Liang et al. [21] investigated the influence of six distinct cases of installing distinct baffles in the triangular grooved ducts on heat transfer by employing a model of  $SST\ k-\omega$ . The resistance of frictional, and coefficient of heat transfer in the Re number range of 1000–6000 were worked, and the baffle influence on the pattern of flow and distribution of temperature was analyzed. It was observed that compared to without baffle, the Nu number increase can be reached 1.5–1.6 times.

As can be seen from the available literature research, the effect of different baffle setups, spacings, and apex angles of the corrugated channels is investigated on heat transfer and flow properties in cross-grooved flow ducts in most of the works. In this study, unlike works in the literature, the influences of placement angles and heights of rectangular baffles in the cross-circular grooved rectangular ducts on heat transfer, flow structure, variations of temperature, pressure drop, PEC number, and TKE are searched. Thus, the most important difference of this study from other studies in the literature is that it specifies the great benefit in terms of the development of engineering systems by determining whether the baffle angle or height is a more effective parameter by means of the detailed examinations on the thermal–hydraulic performances of the cross-circular grooved rectangular flow ducts. The rectangular baffles were placed at the top of the upper rectangular channel at different angles and heights. The study was numerically attained by solving the equations of Navier–Stokes and energy in 3D and steady employing the Ansys-Fluent program with the  $k-\varepsilon$  turbulence model. The circular grooved ducts employed in the work were designed according to the studies in the literature, by asking the flow to move easily in the grooves and the heat transfer to be at the highest level. The temperature of the inlet of the air employed as the working fluid is 293 K ( $T_i$ ), and the duct surfaces with circular grooves are at a constant temperature of 373 K ( $T_s$ ). The Reynolds number (Re), the rectangular baffles angles ( $\varphi$ ) to the top of the section of cross-circular grooved rectangular ducts, and the heights are the variable parameters examined in the study. The investigated range of the Re number is 1000–6000, and the angles and heights of the baffles horizontally to the upper part of the duct are  $30^\circ$ ,  $60^\circ$ , and  $90^\circ$  and  $0.25H$ ,  $0.5H$ , and  $0.75H$ , respectively. However, in the case of a baffle height of  $0.75H$  when using an angle of  $30^\circ$ , the baffle protrudes from the channel, so the baffle height of  $0.75H$  could not have been analyzed at this angle. The results of this work were checked against the numerical and experimental outcomes of the work in the literature and it was attained that the studies were fairly coherent. The results obtained from the work were presented as velocity, TKE, pressure changes, mean Nu number ( $Nu_m$ ) and PEC number along the midpoint of the upper section of the cross-circular grooved rectangular duct, and temperature ( $T$ ) and heat amounts ( $Q$ ) of the fluid at the duct exit for the various baffle angles and heights comparing with the non-baffled case. The fluid contour distributions of velocity, velocity vector, temperature, and TKE for the cross-circular grooved rectangular ducts with and non-baffle were exhibited at Re numbers of 1000 and 6000, respectively.

## 2 Numerical analysis

In this work, the numerical solution of flow and heat transfer with a three-dimensional, steady and turbulence model of  $k-\varepsilon$  of the cross-circular grooved rectangular duct with various angle and height arrangements of the rectangular baffle has been performed by employing the Ansys-Fluent software program, which is the finite volume method.

The convergence criteria are  $10^{-6}$  for the energy equation, and  $10^{-7}$  for the momentum equation. The mean number of iterations is 2,000,000 and the mean time taken to obtain numerical solution results is 5380 s. Besides, the standard  $k-\varepsilon$  turbulence model for cross-circular grooved ducts has been implemented in the computational calculations.

The heat transfer and flow analysis for the cross-circular grooved rectangular duct with the various rectangular baffle angles of placement and heights have been performed by the analysis of equations of partial differential derived from the time-averaged mass, momentum, and energy conservation equations for turbulence flow under the conditions of steady-state where there are not forces of body as identified as follows [22, 23]:

Continuity equation,

$$\frac{\partial \bar{u}}{\partial x} + \frac{\partial \bar{v}}{\partial y} + \frac{\partial \bar{w}}{\partial z} = 0, \quad (1)$$

Equation (1) presents the conservation of continuity (mass) equation of the fluid entering cross-circular grooved rectangular ducts.

Momentum equation.

$x$  momentum equation,

$$\left[ \bar{u} \frac{\partial \bar{u}}{\partial x} + \frac{\partial (\overline{u'^2})}{\partial x} \right] + \left[ \bar{v} \frac{\partial \bar{u}}{\partial y} + \frac{\partial (\overline{u'v'})}{\partial y} \right] + \left[ \bar{w} \frac{\partial \bar{u}}{\partial z} + \frac{\partial (\overline{u'w'})}{\partial z} \right] = -\frac{1}{\rho} \frac{\partial \bar{p}}{\partial x} + \nu \left( \frac{\partial^2 \bar{u}}{\partial x^2} + \frac{\partial^2 \bar{u}}{\partial y^2} + \frac{\partial^2 \bar{u}}{\partial z^2} \right), \quad (2)$$

$y$  momentum equation,

$$\left[ \bar{u} \frac{\partial \bar{v}}{\partial x} + \frac{\partial (\overline{v'^2})}{\partial x} \right] + \left[ \bar{v} \frac{\partial \bar{v}}{\partial y} + \frac{\partial (\overline{v'v'})}{\partial y} \right] + \left[ \bar{w} \frac{\partial \bar{v}}{\partial z} + \frac{\partial (\overline{v'w'})}{\partial z} \right] = -\frac{1}{\rho} \frac{\partial \bar{p}}{\partial y} + \nu \left( \frac{\partial^2 \bar{v}}{\partial x^2} + \frac{\partial^2 \bar{v}}{\partial y^2} + \frac{\partial^2 \bar{v}}{\partial z^2} \right), \quad (3)$$

$z$  momentum equation,

$$\left[ \bar{u} \frac{\partial \bar{w}}{\partial x} + \frac{\partial (\overline{w'^2})}{\partial x} \right] + \left[ \bar{v} \frac{\partial \bar{w}}{\partial y} + \frac{\partial (\overline{w'v'})}{\partial y} \right] + \left[ \bar{w} \frac{\partial \bar{w}}{\partial z} + \frac{\partial (\overline{w'w'})}{\partial z} \right] = -\frac{1}{\rho} \frac{\partial \bar{p}}{\partial z} + \nu \left( \frac{\partial^2 \bar{w}}{\partial x^2} + \frac{\partial^2 \bar{w}}{\partial y^2} + \frac{\partial^2 \bar{w}}{\partial z^2} \right), \quad (4)$$

Momentum equations in the  $x$ ,  $y$ , and  $z$  directions are shown for the cross-circular grooved rectangular ducts in Eqs. 2, 3, and 4, respectively.

Energy equation,

$$\left[ \bar{u} \frac{\partial \bar{T}}{\partial x} + \bar{v} \frac{\partial \bar{T}}{\partial y} \right] + \bar{w} \frac{\partial \bar{T}}{\partial z} + \frac{\partial (\overline{u'T'})}{\partial x} + \frac{\partial (\overline{v'T'})}{\partial y} + \frac{\partial (\overline{w'T'})}{\partial z} = \left( \frac{k}{\rho c_p} \right) \left( \frac{\partial^2 \bar{T}}{\partial x^2} + \frac{\partial^2 \bar{T}}{\partial y^2} + \frac{\partial^2 \bar{T}}{\partial z^2} \right), \quad (5)$$

Equation 5 indicates the energy equation for the cross-circular grooved rectangular duct

Turbulence kinetic energy equation,

$$\frac{\partial (\rho u k')}{\partial x} + \frac{\partial (\rho v k')}{\partial y} + \frac{\partial (\rho w k')}{\partial z} = \frac{\partial}{\partial x} \left( \frac{\mu_t}{\sigma_k} \frac{\partial k'}{\partial x} \right) + \frac{\partial}{\partial y} \left( \frac{\mu_t}{\sigma_k} \frac{\partial k'}{\partial y} \right) + \frac{\partial}{\partial z} \left( \frac{\mu_t}{\sigma_k} \frac{\partial k'}{\partial z} \right) + \mu_t \phi - \rho \varepsilon, \quad (6)$$

Turbulence viscosity,

$$\mu_t = C_{\mu'} \rho \frac{k'^2}{\varepsilon}, \quad (7)$$

Equations of turbulence kinetic energy and turbulence viscosity ( $\mu_t$ ) of turbulent flow due to the baffles in the channel are given in Eqs. 6 and 7, respectively.

For the turbulence model of  $k$ - $\varepsilon$  employed in the study used by Karabulut [24], when  $\varepsilon$  shows distribution of turbulence,  $k'$  and  $\phi$  indicate the terms of turbulence kinetic energy and viscous dissipation as in Eqs. 8 and 9, respectively.

Turbulence kinetic energy,

$$k' = \frac{1}{2} (\overline{u'^2} + \overline{v'^2} + \overline{w'^2}), \quad (8)$$

Viscous dissipation term,

$$\phi = 2\mu \left[ \left( \frac{\partial u}{\partial x} \right)^2 + \left( \frac{\partial v}{\partial y} \right)^2 + \left( \frac{\partial w}{\partial z} \right)^2 \right] + \mu \left[ \left( \frac{\partial v}{\partial x} + \frac{\partial u}{\partial y} \right)^2 + \left( \frac{\partial w}{\partial y} + \frac{\partial v}{\partial z} \right)^2 + \left( \frac{\partial u}{\partial z} + \frac{\partial w}{\partial x} \right)^2 \right] \quad (9)$$

Turbulence kinetic energy disappearance equation,

$$\frac{\partial (\rho u \varepsilon)}{\partial x} + \frac{\partial (\rho v \varepsilon)}{\partial y} + \frac{\partial (\rho w \varepsilon)}{\partial z} = \frac{\partial}{\partial x} \left( \frac{\mu_t}{\sigma_\varepsilon} \frac{\partial \varepsilon}{\partial x} \right) + \frac{\partial}{\partial y} \left( \frac{\mu_t}{\sigma_\varepsilon} \frac{\partial \varepsilon}{\partial y} \right) + \frac{\partial}{\partial z} \left( \frac{\mu_t}{\sigma_\varepsilon} \frac{\partial \varepsilon}{\partial z} \right) + C_{1\varepsilon} \mu_t \frac{\varepsilon}{k'} - C_{2\varepsilon} \rho \frac{\varepsilon}{k'} \quad (10)$$

Turbulence kinetic energy disappearance equation is pointed out in Eq. 8 employed to solve  $k-\varepsilon$  turbulence model, and also  $C_{\mu}$ ,  $C_{1\varepsilon}$ ,  $C_{2\varepsilon}$ ,  $\sigma_k$ , and  $\sigma_\varepsilon$  which are constants of model are the typical values of default used in the standard  $k-\varepsilon$  turbulence model [22]. These constant values were achieved by numerous data-fitting iterations for many turbulence flows.

Re number is figured out by the given Eq. 11 [19, 23, 24],

$$Re = \frac{V_\infty D_h}{\nu}, \tag{11}$$

$D_h$  is the hydraulic diameter of the jet inlet as shown in Eq. 12 [19, 23, 24],

$$D_h = \frac{4A_c}{P}, \tag{12}$$

The Nu number is characterized to be a rate of the convection heat transfer rate to the conduction heat transfer in Eq. 13 as given as follows [25]:

$$-k \left( \frac{\partial T}{\partial n} \right)_s = h \Delta T_{lm} \text{ and } Nu = \frac{hL}{k}, \tag{13}$$

Here,  $h$  is the coefficient of local heat transfer on the plane,  $n$  is the vertical direction to the surface and the local Nu number is computed as above.

The temperature difference of logarithmic ( $\Delta T_{lm}$ ) between the wall surface of the circular grooves and fluid is computed by Eq. 14 [3],

$$\Delta T_{lm} = \frac{(T_i - T_o)}{\ln \left( \frac{T_w - T_i}{T_w - T_o} \right)}, \tag{14}$$

where  $T_i$ ,  $T_o$ , and  $T_w$  are the temperatures of the entry and exit of the fluid and the temperature of the wall surface of the circular grooves, respectively.

Mean heat transfer coefficient ( $h_m$ ) [25],

$$h_m = \frac{1}{L} \int_0^L h dx, \tag{15}$$

Mean Nu number ( $Nu_m$ ) [25],

$$Nu_m = \frac{h_m L}{k}, \tag{16}$$

Mean heat transfer coefficient ( $h_m$ ) and mean Nu number ( $Nu_m$ ) are calculated by Eqs. 15 and 16 along the cross-circular grooved surfaces of the rectangular duct, respectively.

Pressure drop ( $\Delta p$ ) is calculated with Eq. 17 between the cross-circular grooved rectangular duct inlet and exit [3],

$$\Delta p = \frac{f \rho L}{2 D_h} u_m^2, \tag{17}$$

where  $f$  is the friction factor and  $L$  is the length of the duct.

PEC (Performance Evaluation Criterion) number [17],

$$PEC = \frac{Nu_m \text{ duct with baffles} / Nu_m \text{ duct without baffles}}{(\Delta p_{\text{duct with baffles}} / \Delta p_{\text{duct without baffles}})}, \tag{18}$$

PEC number is a thermal-hydraulic performance indicator that indicates the increase in pressure drop ( $\Delta p$ ) against the increase in Nu number ( $Nu_m$ ) in ducts with fins compared to ducts without fins and is calculated with Eq. 16.

The dimensionless duct length variable ( $z^*$ ) is described as shown in Eq. 17,

$$z^* = \frac{z}{L} \tag{19}$$

where  $z$  displays the local channel length.

### 3 Geometric model

Projection view of the cross-circular grooved rectangular duct having baffle and boundary conditions employed in the analyses are given in Fig. 1. A mesh structure of tetrahedral was employed for the simulations as the proper duct type and exhibited in Fig. 2.

While the length,  $L$ , and width,  $W$  of the cross-grooved duct are 70.71 mm and 8.165 mm, respectively, duct height,  $H$ , and space between two baffles,  $d$ , are 7.071 mm and 8.165 mm, respectively. Besides, the employed rectangular baffle heights are  $0.25H$ ,  $0.5H$ , and  $0.75H$ . However, the range of entry velocity of the air changes with  $2.25 \text{ ms}^{-1}$  ( $Re = 1000$ )- $13.50 \text{ ms}^{-1}$  ( $Re = 6000$ ). A

**Fig. 1** Projection view of the cross-circular grooved rectangular duct having baffle and boundary conditions

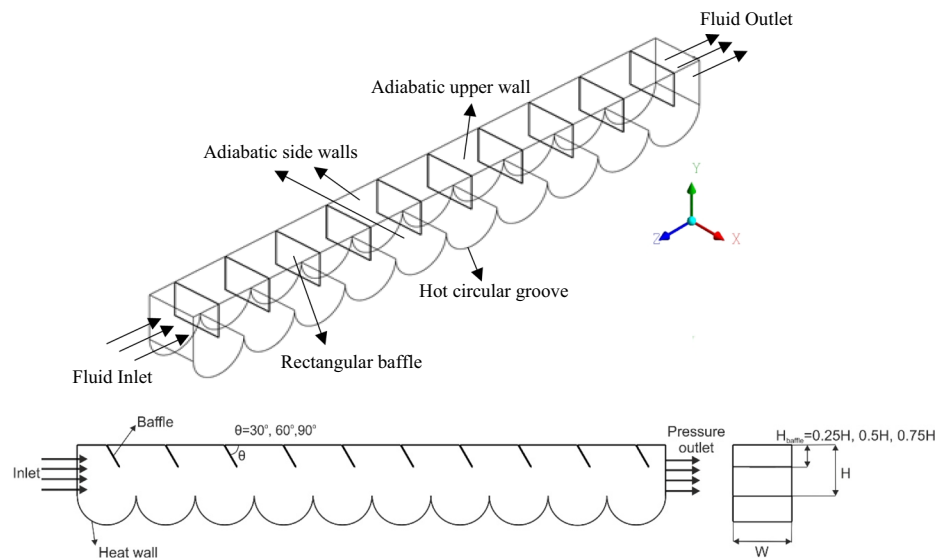
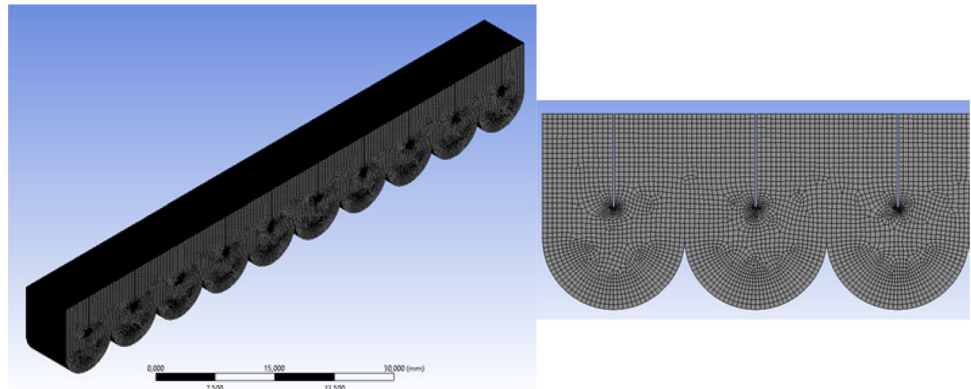


**Fig. 2** Mesh structure of the cross-circular grooved rectangular duct



constant radius of 4.0825 mm for circular grooved is employed depending on the channel length. There are ten rectangular baffles in the upper part of the rectangular duct, which are formed according to the dimensions of the ducts found in the literature, and ten circular grooves in the lower part. Also, as a boundary condition, a fixed temperature of 373 K is implemented to the circular surfaces of the grooved duct, while the air temperature entering the rectangular duct at the top is 293 K. Besides, velocity inlet and pressure outlet boundary conditions are applied at the duct inlet and outlet, respectively. The upper and side walls are adiabatic. However, this work was performed under the following suppositions:

- The domain of the flow is 3D, steady and turbulent for the cross-circular grooved rectangular duct,
- Air employed is incompressible, and its thermal features are fixed,
- Generation of the heat for the air, and the surfaces of the rectangular baffles do not exist.

#### 4 Valuation of the results

The  $Nu_m$  outcomes of the empirical study of Scott and Lobato [27] and the computational results of Liu and Niu [3], Zhang [12], Zhang [28] and Li and Gao [19] are compared with the computational outcomes of this work for triangular grooved ducts with 60° and 90° apex angles and non-baffle are indicated in Fig. 3a and b respectively. Comparisons of the computational outcomes of Zhang [12] and Zhang [28] performed by employing a turbulence model of  $k-\omega$  with a low Re number and Li and Gao [19] implemented employing the turbulence model of  $k-\varepsilon$  and this work are indicated in Fig. 3a for the grooved duct with the angle of apex of 60° and non-baffled. Figure 3b points out the comparisons of Scott and Lobato [27]'s empirical outcome and the computational outcomes of Liu and Niu [3] performed by employing the model of Reynolds stress, Li and Gao [19] and this work for the grooved duct with an angle of the apex of 90°, and without baffle. For the  $Nu_m$  in Fig. 3a, the highest deviation of this work is 4.82% with computational studies at the 60° apex angle. However, as indicated in Fig. 3b, the differences between the experimental outcomes of Scott and Lobato [27] and the computational outcomes of this work are within 3.53% for an apex angle of 90°. Therefore, the agreement level of this study performed by employing the turbulence model of  $k-\varepsilon$  with the computational and empirical works is considered to be

**Fig. 3** Comparing the  $Nu_m$  outcomes of the empirical and computational with the outcomes of this study for the apex angles of **a**  $60^\circ$ , **b**  $90^\circ$

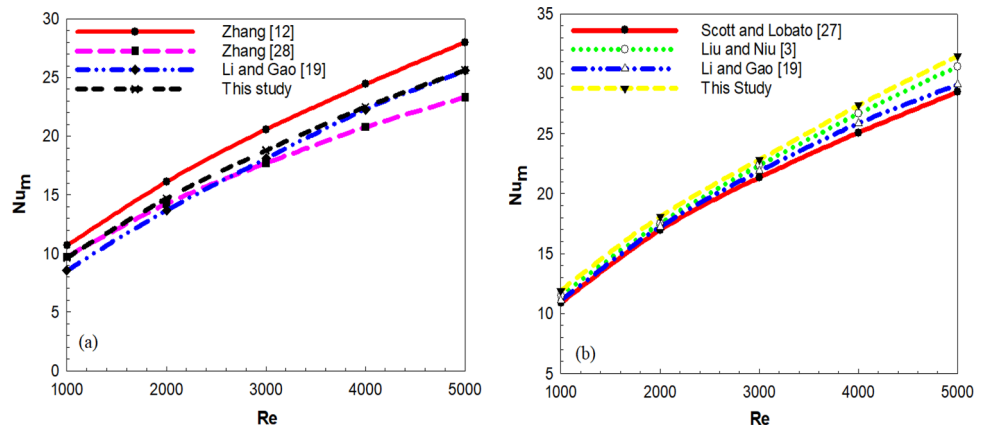


**Table 1** Grid independence test results considering the  $Nu_m$  for the grooved duct non-baffle

Mesh numbers	Re = 1000 $Nu_m$	Re = 2000 $Nu_m$	Re = 3000 $Nu_m$	Re = 6000 $Nu_m$
450,571	9.1025	14.823	19.5614	30.985
957,842	9.1095	14.8294	19.5704	31.001
<b>1,184,080</b>	<b>9.11</b>	<b>14.83</b>	<b>19.57</b>	<b>31.001</b>
1,254,150	9.1120	14.9804	19.5725	31.0015

acceptable and consistent with each other and hence is employed for various baffle angles and heights, and channel set-ups at this work.

Grid independence tests in order to specify the influence of number of grid on the  $Nu_m$  for the grooved duct surfaces non-baffled at various Re number values are pointed out in Table 1. The attained results displayed that grid elements of 1,184,080 are sufficient for the corrugated duct non-baffled. In addition, 2,587,450 grid elements were used for the cross-circular corrugated rectangular duct with rectangular baffles.

In Fig. 4A and B, the velocity contour distributions of circular grooved rectangular ducts non-baffle, and with baffle angles of  $30^\circ$ ,  $60^\circ$ , and  $90^\circ$ , and baffle heights of  $0.25H$ ,  $0.5H$ , and  $0.75H$  are shown for distinct Re numbers of A-Re = 1000 and B-Re = 6000, respectively. In the without baffle duct, the direct contact of the fluid entering the duct with the circular groove is quite low and the fluid leaves the duct directly. When baffles are added to the duct, the fluid can be directed to the grooves. Although this orientation increases with the increase of the baffle angle, it becomes especially evident with the increase in the baffle height. While jet flow-like flow characteristics occur along the duct at  $60^\circ$  and  $90^\circ$  baffle angles at  $0.75H$  baffle height, the most movement of fluid in circular grooved ducts is obtained at a baffle angle of  $90^\circ$  and height of  $0.75H$ , which has an increasing influence on heat transfer. In addition, the increase in the baffles' height ensures the fluid's movement between the baffles. However, by raising the Re number to 6000, the flow-activating effect of the baffles on the circular grooves increases, further improving the heat transfer.

The distributions of the velocity vector contour for the first five circular grooves and Re numbers of A-Re = 1000 and B-Re = 6000 of the circular grooved rectangular ducts non-baffle, and with  $30^\circ$ ,  $60^\circ$ , and  $90^\circ$  baffle angles, and  $0.5H$  and  $0.75H$  baffle heights where vector densities are higher than  $0.25H$  are given in Fig. 5A and B, respectively. In the without baffle, since the fluid moves along the top half of the duct toward the duct outlet, the fluid movement in the circular grooves is very low. In addition, small clockwise vortex movements occur in the circular grooves. When  $30^\circ$  angled baffles are added to the upper part of the grooved duct; while the fluid motion in the upper half of the duct moves similar to the one without baffle, the fluid motion intensifies at the entrance of the circular grooves and clockwise vortices are formed there. When the baffle length is increased to  $0.5H$  at the same angle, the intensity of vortex formation in the grooves increases. In addition, counterclockwise vortices occur between the baffles. When the baffle angle is increased to  $60^\circ$ , it has been observed that fluid mobility increases both between the baffles and in the grooves, especially at  $0.5H$  and  $0.75H$  baffle heights. At the  $90^\circ$  angle of the baffle and the height of  $0.75H$ , the vortex motion in the circular grooves reaches a maximum level, since the fluid velocity between the baffle endpoint and the top of the groove exhibits a jet flow-like motion. When the Re number is increased to 6000, although there are similar fluid movements in the circular grooves and the duct, the velocity of the fluid and hence the intensities and densities of the velocity vectors increase.

The distributions of temperature contours in the rectangular ducts with circular grooved non-baffle and with baffle having distinct placement angles of  $30^\circ$ ,  $60^\circ$ , and  $90^\circ$ , and heights of  $0.25H$ ,  $0.5H$ , and  $0.75H$  at A-Re = 1000 and B-Re = 6000 are illustrated in Fig. 6A and B, respectively. Compared to the temperature contour distribution in the without baffle state, the temperature gradient increases due to the turbulence intensity created by the addition of baffles to the circular grooved ducts. When the baffle height is increased to  $0.75H$ , the increase in fluid temperatures toward the end of the ducts is the clearest evidence of this situation. Thus, while cooling increases in circular grooves, the temperature gradient in the duct above the circular grooved section gets better,

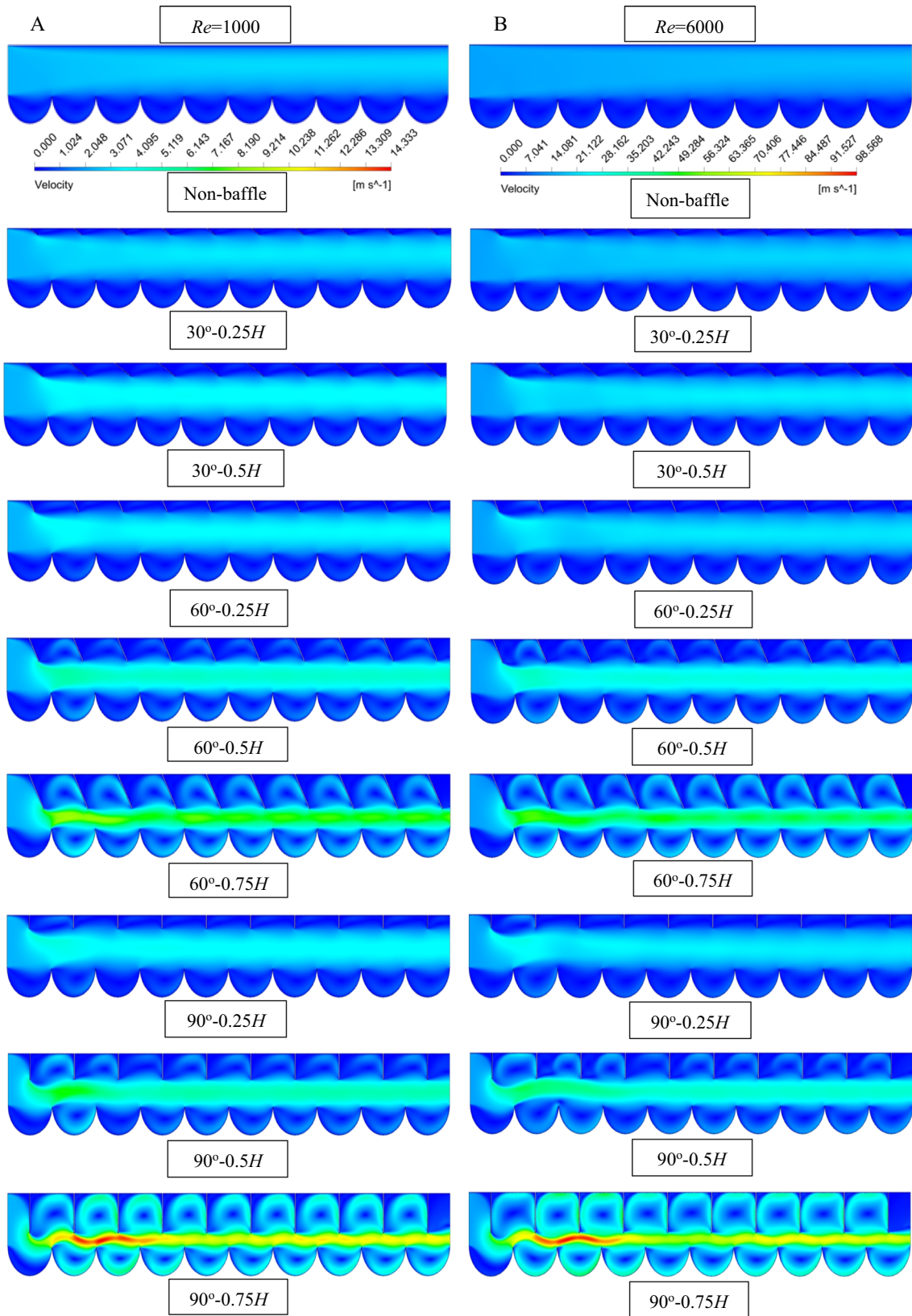


**Fig. 4** Velocity contour distributions of circular grooved rectangular ducts non-baffle, and with baffle angles of 30°, 60°, and 90°, and heights of 0.25H, 0.5H, and 0.75H for distinct Re numbers of **A**-Re = 1000, **B**-Re = 6000



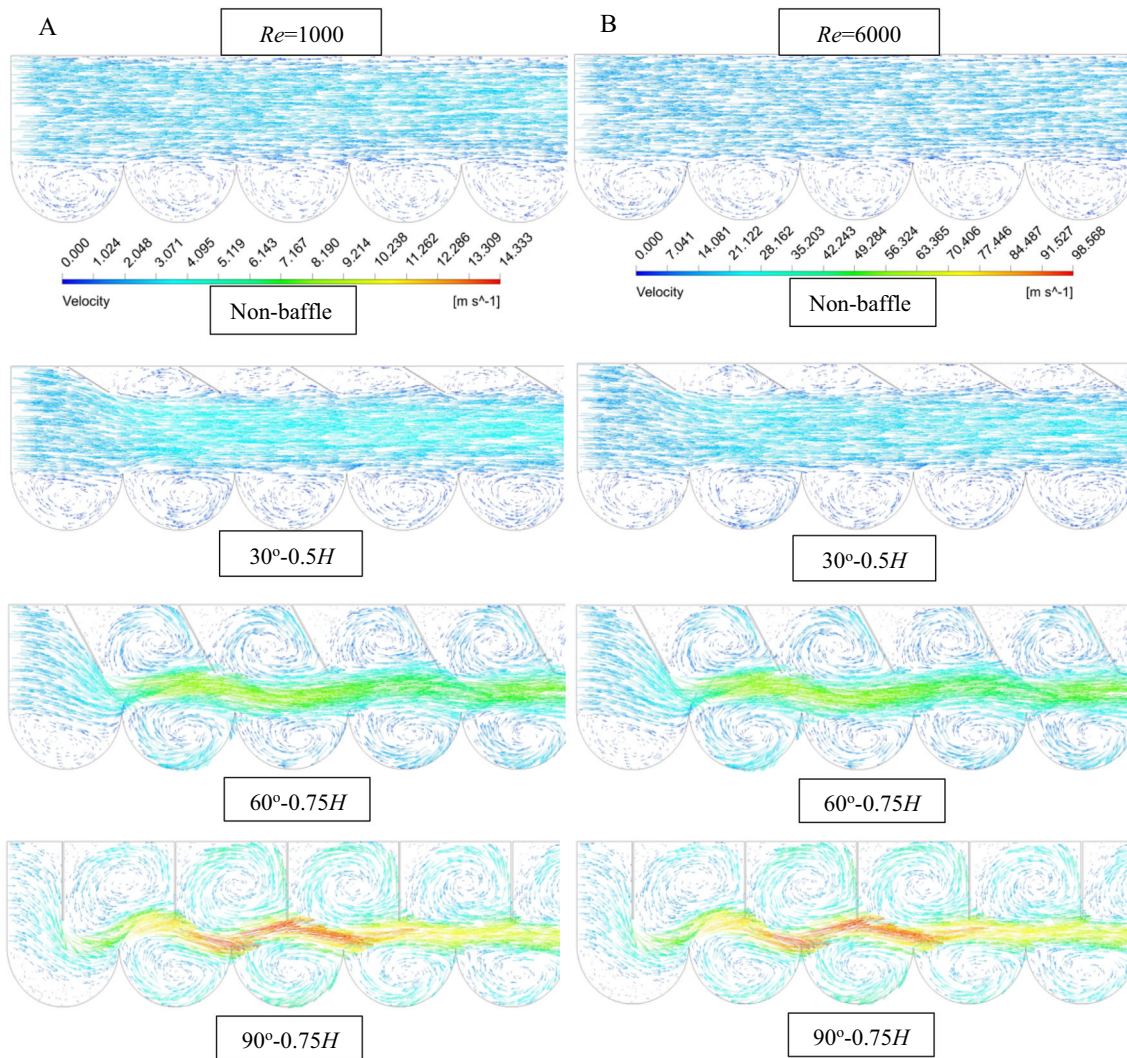


**Fig. 5** Velocity vector contour distributions of circular grooved rectangular ducts non-baffle, and with baffle angles of 30°, 60°, and 90°, and baffle heights of 0.5H and 0.75H for distinct Re numbers of **A**-Re = 1000, **B**-Re = 6000

especially in the case of 0.75H height and 90° baffle angle. However, for Re = 6000, the heat transfer is much in evidence due to the increased vortex effect in circular grooves.

Turbulence kinetic energy contour distributions of circular corrugated rectangular ducts non-baffle, and with baffle angles of 30°, 60°, and 90°, and various baffle heights of 0.25H, 0.5H, and 0.75H are shown in Fig. 7A and B for the A-Re = 1000 and B-Re = 6000 values, respectively. As observed in Fig. 7A and B, the turbulence kinetic energy level increases because of the turbulence created in the circular grooved ducts with baffled depending on the mixing ratio in the fluid. Depending on the increase in the baffle angle and height, the turbulence intensity increases at the baffle tips and circular groove entrances; increasing the Re number also improves the kinetic energy exchange in the grooves. However, while the greatest change in turbulent kinetic energy is seen in ducts where the baffle angle is 90° and the baffle height is 0.75H, it can be determined from the contour distribution that turbulent flows are more severe in the duct where the Re number is 6000.

The fluid temperature variation taken along the midpoints of the upper parts of the circular grooved rectangular ducts non-baffle, and with baffle angles of 30°, 60°, and 90°, and baffle heights of 0.25H, 0.5H, and 0.75H are given according to the variation of the Re numbers in Fig. 8. The temperature of the fluid entering the grooved ducts increases according to the amount of contact with the hot grooves thanks to the baffles and the degree of turbulence created in the duct. However, increasing the baffle’s angle and height allows the fluid to be better directed into the circular grooves. Fluctuations in temperature seen from the  $Z^* = 0.1-0.4$  parts of the ducts starting from the 0.25H-60° to 0.75H-90° baffled duct are due to the movement of the fluid impinging the first row of baffle in the duct after the first circular groove. While the highest temperature fluctuation seen in this part of the duct is in the baffled duct with 0.5H-90°, these changes in temperature compared to the non-baffle duct are a result of the enhancement in the transfer of heat.

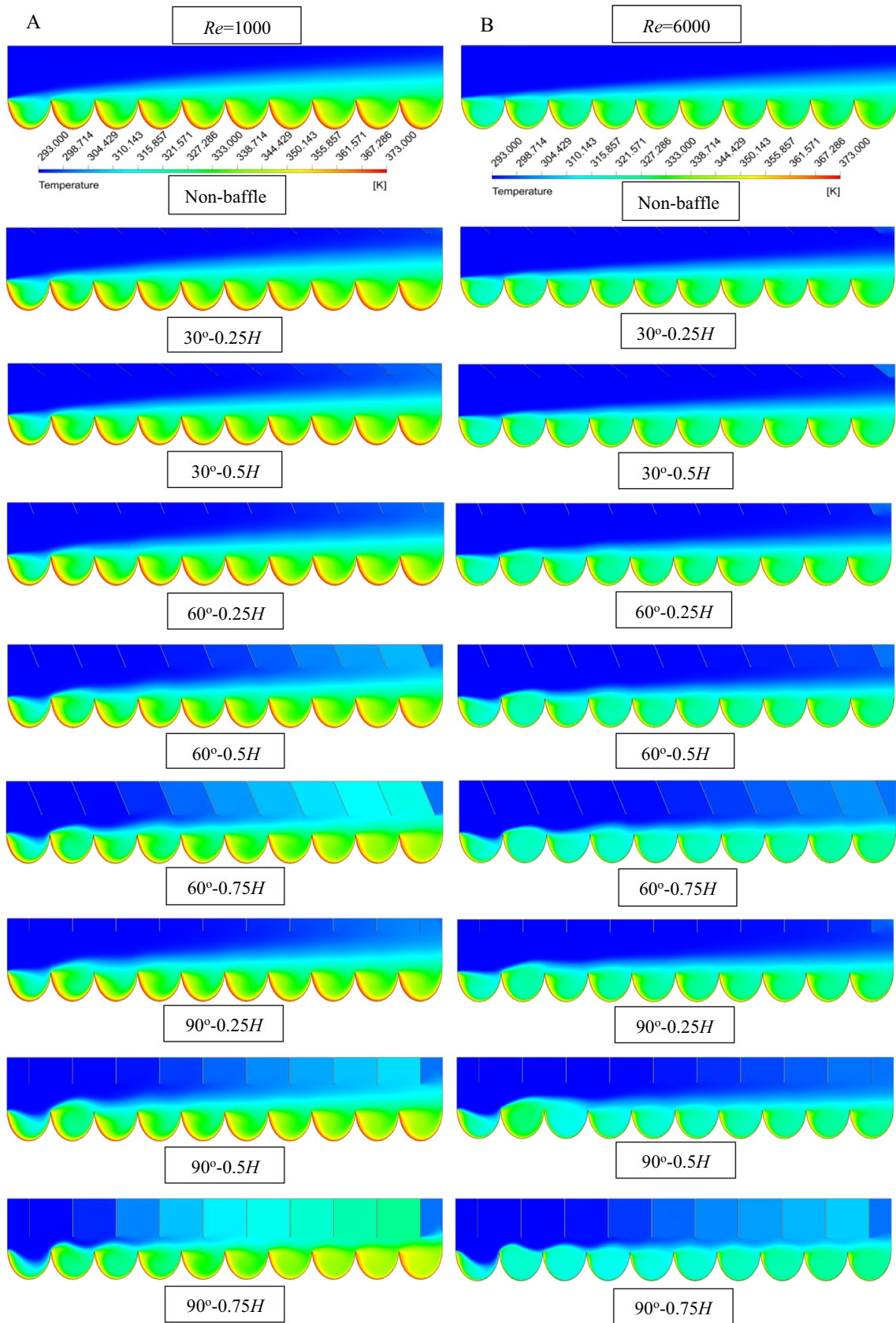


**Fig. 6** Temperature contour distributions of circular grooved rectangular ducts non-baffle, and with baffle angles of 30°, 60°, and 90°, and baffle heights of 0.25H, 0.5H, and 0.75H for distinct Re numbers of **A**-Re = 1000, **B**-Re = 6000

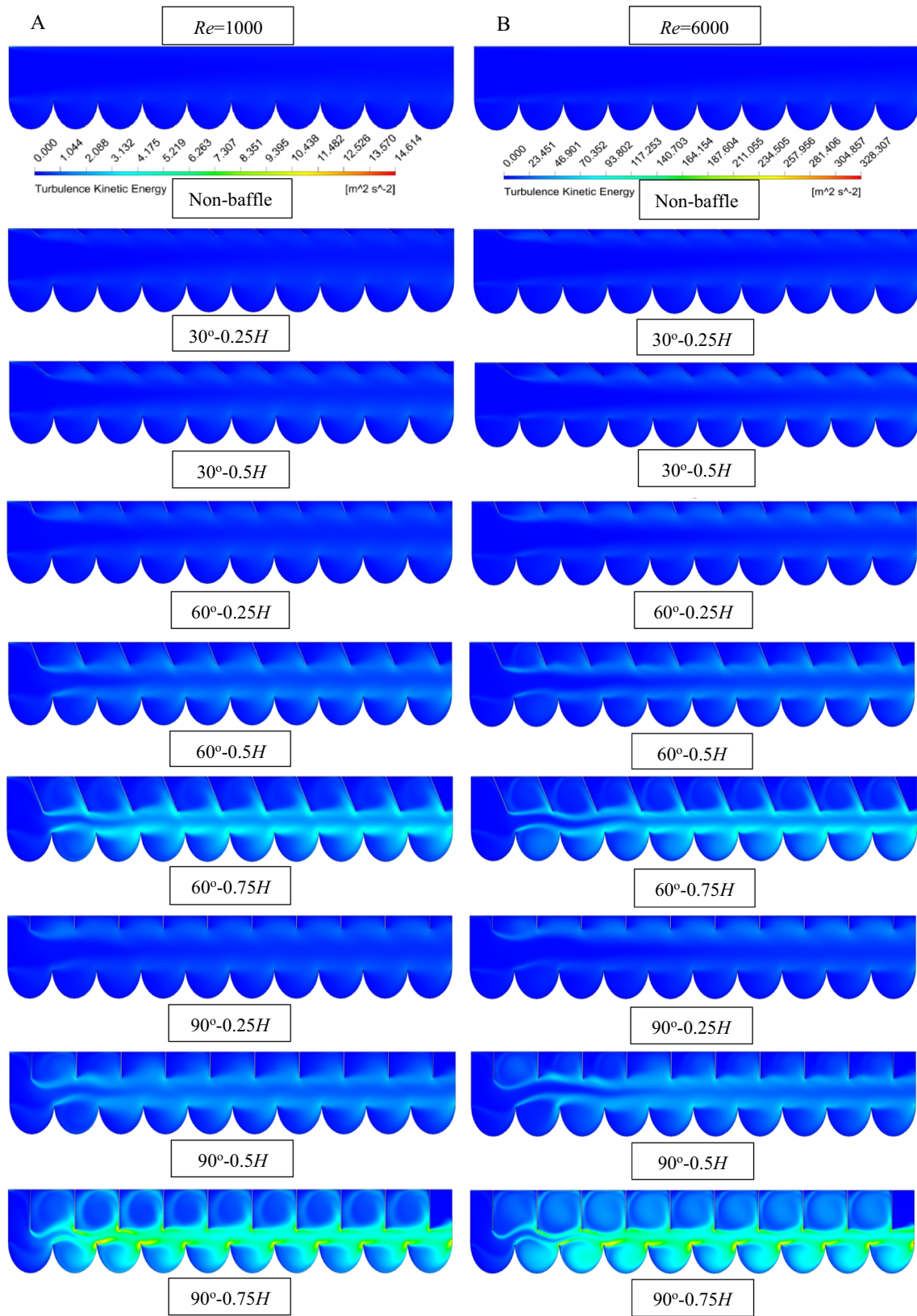


**Fig. 7** Turbulence kinetic energy contour distributions of circular grooved rectangular ducts non-baffle, and with baffle angles of 30°, 60°, and 90° and, baffle heights of 0.25H, 0.5H, and 0.75H for distinct Re numbers of **A**-Re = 1000, **B**-Re = 6000

**Fig. 8** Fluid temperature variations along the upper midpoints parts of circular grooved rectangular ducts non-baffle, and with baffle angles of 30°, 60°, and 90°, and baffle heights of 0.25H, 0.5H, and 0.75H for distinct Re numbers

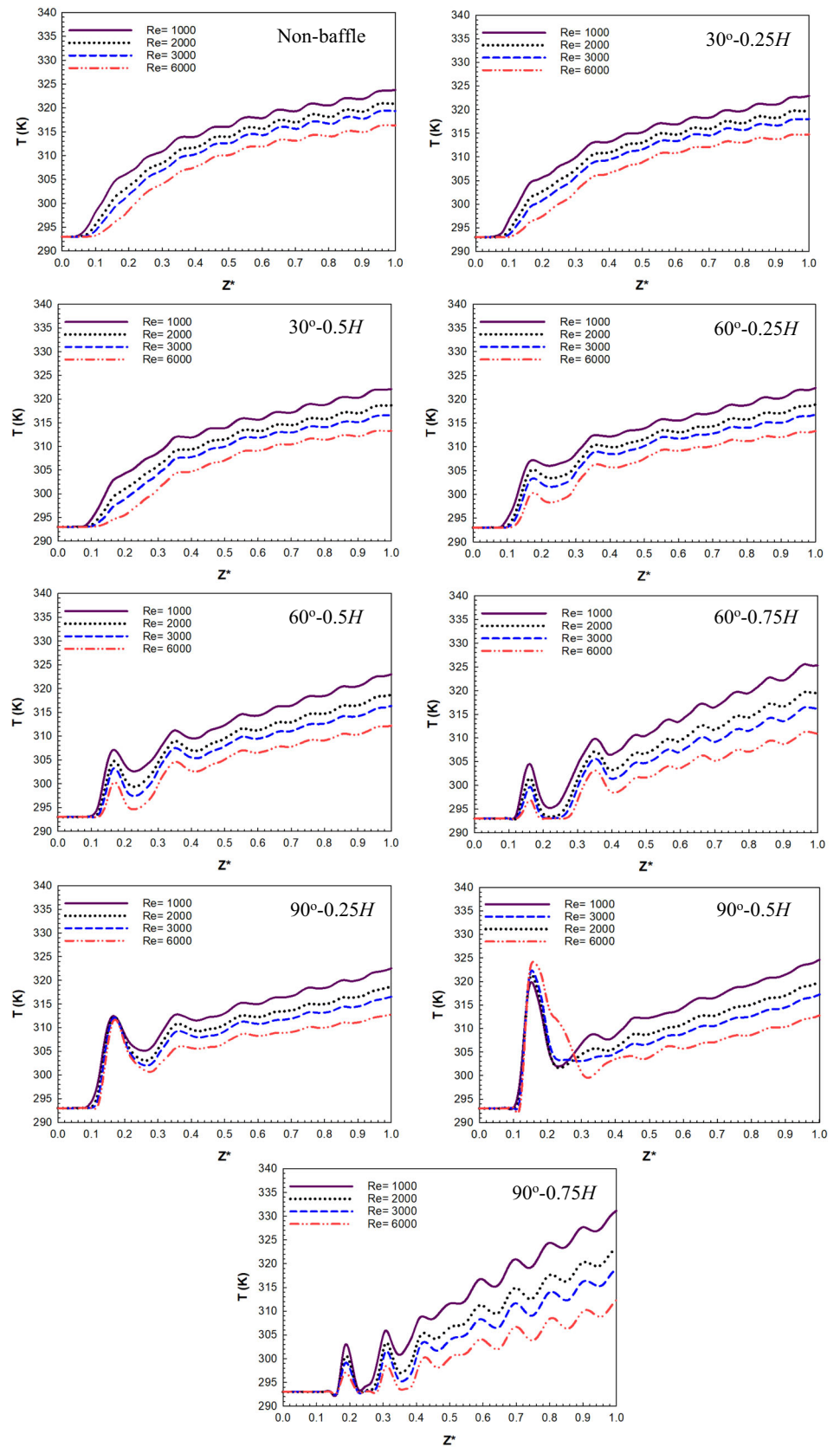
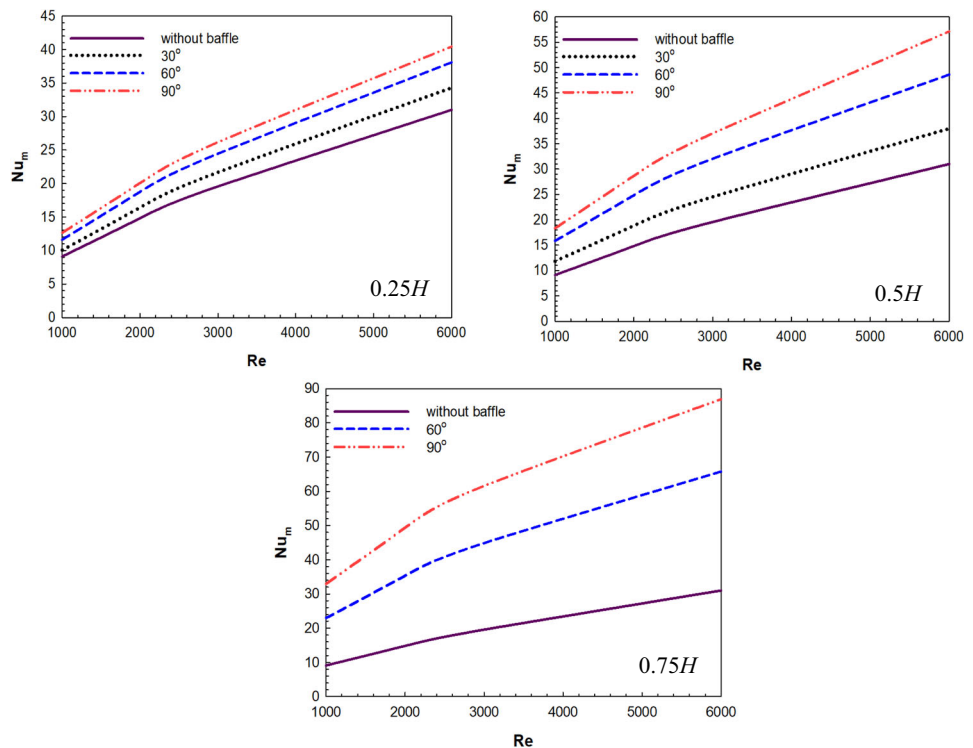


**Fig. 9** Mean  $Nu_m$  variations of circular grooved rectangular ducts non-baffle, and with baffle angles of  $30^\circ$ ,  $60^\circ$ , and  $90^\circ$  for the baffle heights of  $0.25H$ ,  $0.5H$ , and  $0.75H$



The mean  $Nu_m$  variations versus  $Re$  numbers for the rectangular ducts non-baffle and baffle angles of  $30^\circ$ ,  $60^\circ$ , and  $90^\circ$  are shown in Fig. 9 depending on the baffle heights of  $0.25H$ ,  $0.5H$ , and  $0.75H$ . As can be observed in Fig. 9 with the rise of the  $Re$  number, the  $Nu_m$  also increases depending on the heat transfer enhancement from the circular groove ducts. For all three baffle heights, while the  $Nu_m$  rises with the rise of the baffle angle compared to the without baffle situation, the highest  $Nu_m$  value is reached at  $90^\circ$  angle and  $0.75H$  height. For  $Re = 6000$ , the number of  $Nu_m$  increases by 180.48% in the duct with a  $90^\circ$  angle and  $0.75H$  baffle height compared to the duct without a baffle. Also, when compared with the same  $Re$  number ( $Re = 6000$ ) and angle value ( $90^\circ$ ), the  $Nu_m$  increment rate at  $0.75H$  baffle height is 150.02% compared to  $0.25H$  height due to the vortex movements created by rectangular baffles.

Variations of heat transfer ( $Q$ ) values taken exit of the grooved rectangular ducts from the warm surfaces of the circular grooves to fluid are pointed out in Fig. 10 for the baffle heights of  $0.25H$ ,  $0.5H$ , and  $0.75H$ , and distinct baffle angles of  $30^\circ$ ,  $60^\circ$ , and  $90^\circ$ . The vortex movements that occur in the duct due to the placement arrangements of the baffles to the duct affect the improvement in the  $Q$  to the fluid. Besides, as the increase in  $Re$  number will intensify the movements of these vortices in the circular grooves of the duct, the amount of heat transfer to the fluid also increases. For  $Re = 3000$ , an increase of 53.42% and 87.33% in  $Q$  value is obtained in ducts with a  $60^\circ$  angle and  $0.75H$  height of the baffle compared to ducts with  $0.5H$  and  $0.25H$  baffle height, respectively. Considering the 13% increase in heat transfer at a  $Re$  number of 10,000 in the works reached in the literature (Ajeel et al. [29, 30]), it can be said that the baffle arrangements used in the circular grooved ducts in this study are suitable for increasing heat transfer.

In Fig. 11, the variations of the outlet temperature values of the fluid in the circular grooved rectangular ducts non-baffle, and different rectangular baffle angles of  $30^\circ$ ,  $60^\circ$ , and  $90^\circ$ , and heights of  $0.25H$ ,  $0.5H$ , and  $0.75H$  according to  $Re$  number. Depending on the enhancement in the  $Q$  from the circular grooved duct surfaces, the outlet temperature value of the fluid increases. In addition, while the  $Q$  rises with the rise of the  $Re$  number (Fig. 10), the outlet values of the fluid temperature decrease. However, it is observed that the highest value of temperature is attained in the baffled duct with an angle of  $90^\circ$  and a height of  $0.75H$ , while the lowest values for all three cases are obtained in the non-baffle condition.

In Fig. 12, the variations of turbulence kinetic energy (TKE) with  $Re$  number are given along the midpoint of the upper part of the circular grooved rectangular ducts non-baffle, and with different baffle angles of  $30^\circ$ ,  $60^\circ$ , and  $90^\circ$ , and baffle heights of  $0.25H$ ,  $0.5H$ , and  $0.75H$ . The vortices, which are formed as a result of the turbulent movements to be produced in the ducts thanks to the baffles, increase the contact of the fluid with the grooves and the mixing, thus increasing the heat transfer. In parallel with the rise in the  $Re$  number, the turbulence intensity in the baffle tips and between them, and also in the circular grooves enhances with the enhancement in the angle and height of the baffles in the duct. Accordingly, while the cooling of the grooves in the duct improves, pressure drop increases. In particular, for the 6000 value of  $Re$ , the baffle angle of  $90^\circ$  and the height of  $0.75H$  intensify the TKE at the maximum level. The fluctuations seen in TKE (Fig. 12) are due to vortex movements caused by turbulence. For  $Re = 6000$ , the mean TKE value in a duct with a  $90^\circ$  baffle angle and  $0.25H$  height is 97.12% higher than in the duct without a baffle. This value

**Fig. 10** Heat transfer ( $Q$ ) variations of circular grooved rectangular ducts non-baffle, and with baffle angles of  $30^\circ$ ,  $60^\circ$ , and  $90^\circ$  for the baffle heights of  $0.25H$ ,  $0.5H$ , and  $0.75H$

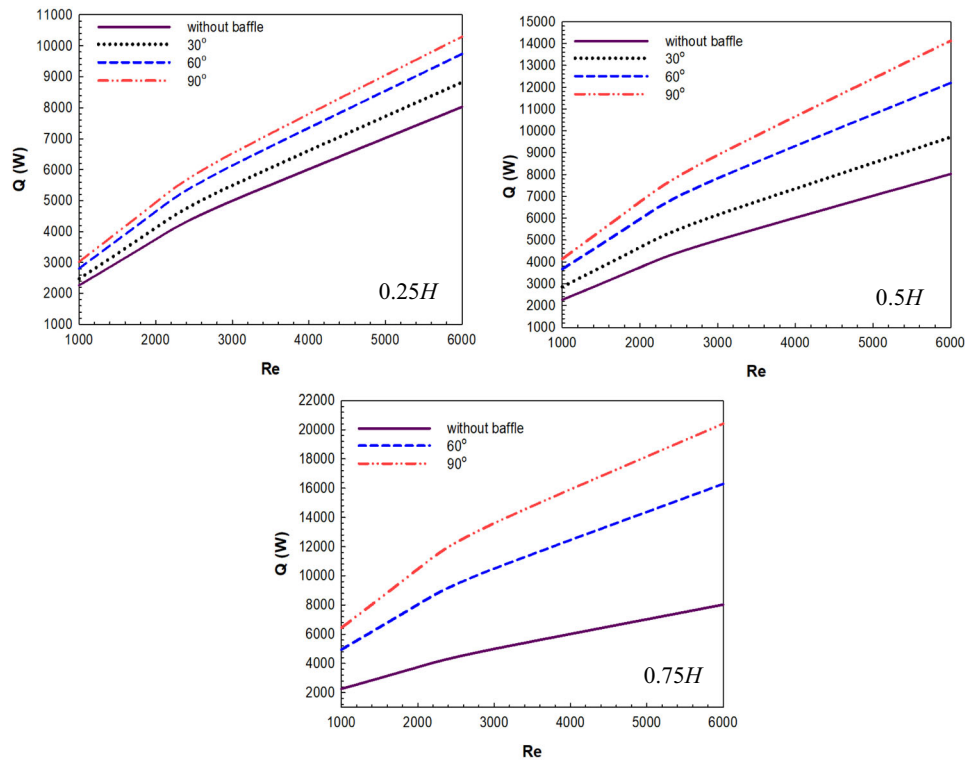
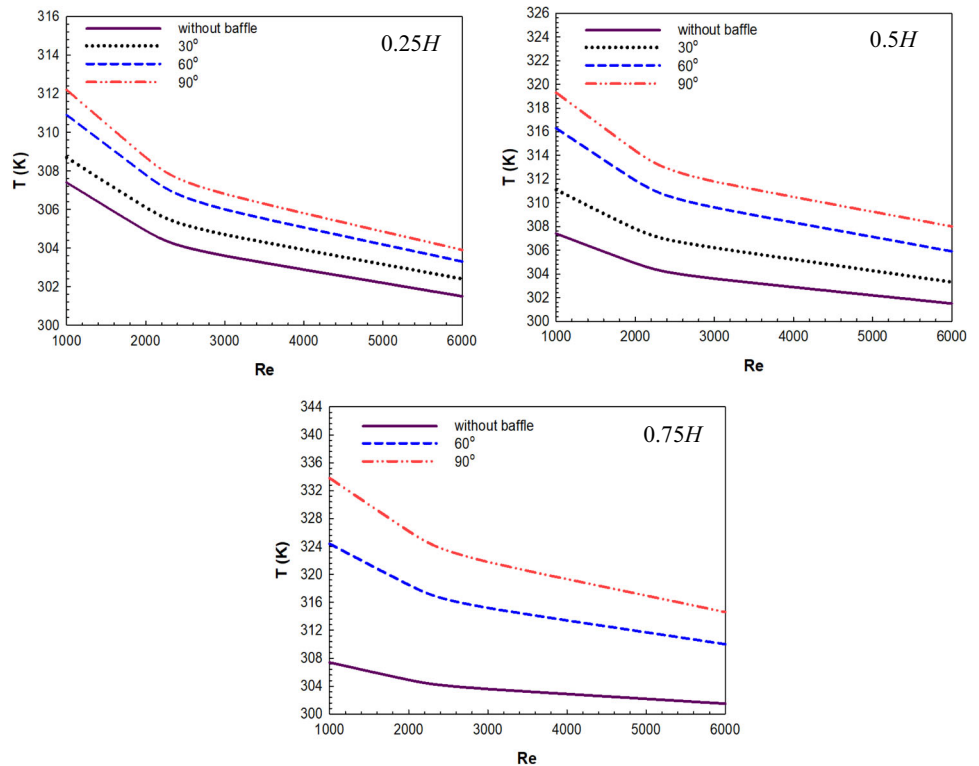
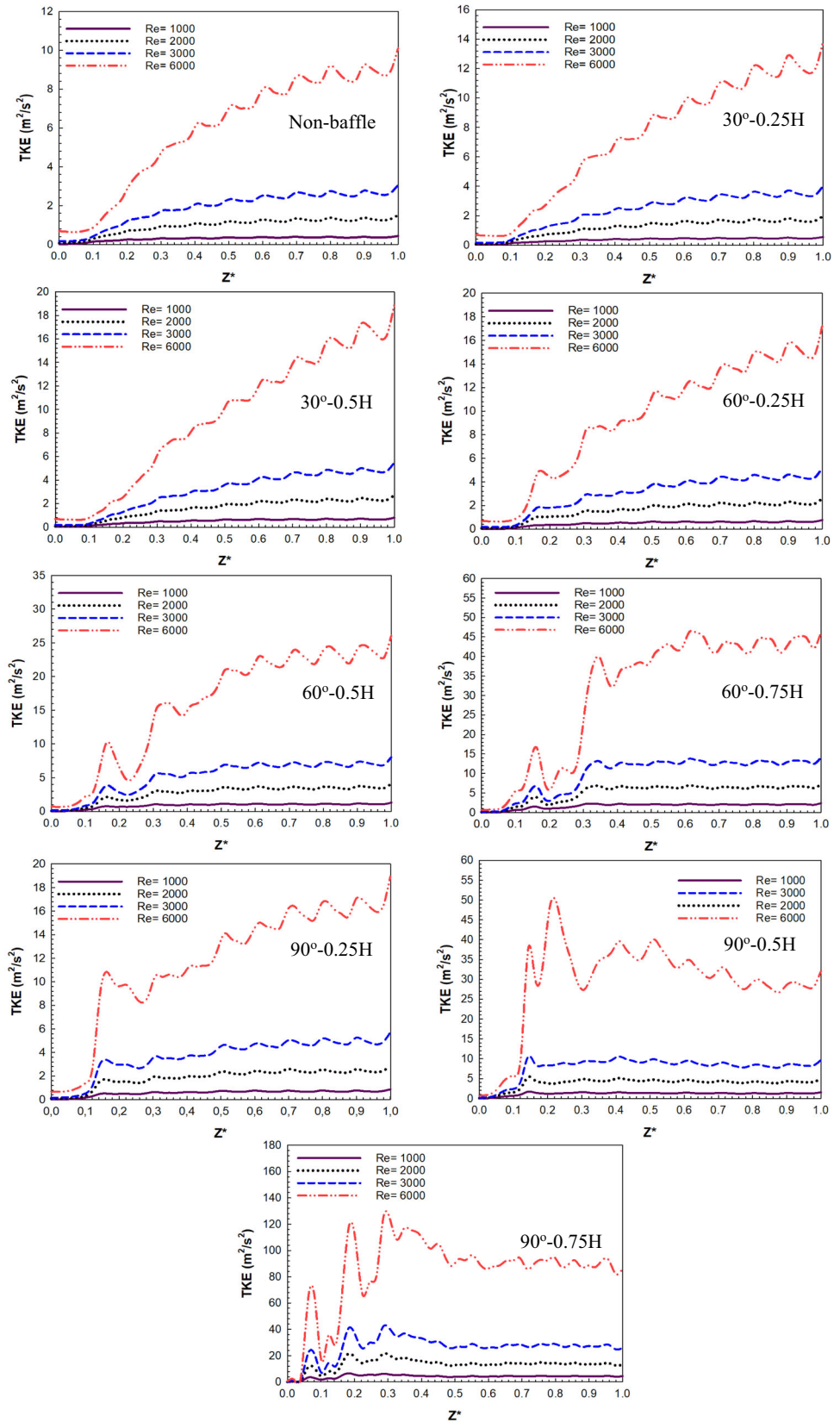


**Fig. 11** Fluid outlet temperature variations of circular grooved rectangular ducts non-baffle, and with baffle angles of  $30^\circ$ ,  $60^\circ$ , and  $90^\circ$  for the baffle heights of  $0.25H$ ,  $0.5H$ , and  $0.75H$



increases to higher values when the baffle height is increased. In the duct with  $0.5H$  baffle height and  $90^\circ$  angle, and  $Re$  number of 6000, the increase in TKE value is 393.8% compared to the non-baffle duct. Moreover, when the baffle angle value is reduced from  $90^\circ$  to  $30^\circ$  at a baffle height of  $0.25H$  for the same  $Re$  number ( $Re = 6000$ ), the increase in value of the TKE decreases to 24.64%. This proves that the baffle height is more decisive on the increase in TKE.

**Fig. 12** Turbulence kinetic energy (TKE) variations along the upper midpoint parts of circular grooved rectangular ducts non-baffle, and with baffle angles of 30°, 60°, and 90°, and baffle heights of 0.25H, 0.5H, and 0.75H for distinct Re numbers



Pressure variations versus Re numbers along the upper midpoint part of the circular grooved rectangular ducts non-baffle, and with different baffle angles of 30°, 60°, and 90°, and baffle heights of 0.25H, 0.5H, and 0.75H are displayed in Fig. 13. Since the

baffle prevents the flow by decreasing the area of the flow cross section at the inlet of duct, higher pressure values are obtained at the inlet in baffled ducts than in the non-baffled. However, while the pressure values decrease from the entrance to the exit of the circular grooved ducts, they increase with the rise in the Re number. The highest drop of pressure is attained in the circular grooved duct with a  $90^\circ$  baffle angle and  $0.75H$  height considering all baffle arrangements. There are fluctuations in the pressure values in the ducts depending on the baffle angle and height. The difference of pressure between the duct entry and exit is obtained with 9534 Pa for  $Re = 6000$  and  $90^\circ$  angle and  $0.75H$  baffle height. At the same Re number ( $Re = 6000$ ), the pressure drop between the entry and exit of the duct without baffle is 79.31 Pa.

While corrugated duct arrangements provide an increase in heat transfer, they cause a rise in pressure drop. Therefore, an effective evaluation of this arrangement is possible by evaluating its thermal–hydraulic performance. Performance Evaluation Criterion (PEC) number can be interpreted grooved duct with a baffle by comparing it to a grooved duct without a baffle ([26]).

In Fig. 14, the variations of PEC number values versus Re number are illustrated at various baffle angles of  $30^\circ$ ,  $60^\circ$ , and  $90^\circ$ , and baffle heights of  $0.25H$ ,  $0.5H$ , and  $0.75H$ . As the baffle angle and height increase, the PEC values decrease because the pressure drops in the ducts enhance. The rise in the Re number also causes a decrease in PEC values as it increases the  $\Delta p$ . However, since the rise in the value of the  $Nu_m$  number is higher against the  $\Delta p$ , it is determined that the best value of PEC is reached in the circular grooved duct with an angle of baffle of  $30^\circ$  and a height of  $0.25H$ . For  $Re = 6000$  and  $30^\circ$  baffle angle, the PEC value at  $0.25H$  baffle height is 66.88% higher than that in the  $0.5H$ . These increment value reaches much higher level when compared a  $90^\circ$  angle and a baffle height of  $0.75H$  with  $30^\circ$  and  $0.25H$ . Therefore, while the lowest PEC number value is obtained for the duct with  $0.75H$  baffle height and  $90^\circ$  angle, the highest PEC value is reached in the case with  $30^\circ$  angle and  $0.25H$  baffle height. However, this result shows that while the increments in baffle angle and height increase the  $Nu_m$  number, they reduce the thermal–hydraulic performance of the grooved ducts. Thus, it is necessary to consider the number of PEC to make a full assessment of baffle arrangement effectiveness. In addition, when the graphs are examined, it is seen that the effect of reducing the baffle height is greater than the decrease in the baffle angle on the rise of the PEC number.

## 5 Conclusions and evaluations

In this work, it is purposed to examine the influences of baffles with different angles and heights added to the upper part of circular grooved rectangular ducts on heat transfer, drop of pressure, performance of thermal–hydraulic, turbulent kinetic energy and flow structure. The solution of the work was performed by numerically finding out the equations of Navier–Stokes and energy employing the turbulence model of  $k-\epsilon$  and Ansys-Fluent program, in 3D and steady. As an outcome of this work, the following main outcomes can be reached.

- In the without baffle duct, the direct contact of the fluid entering the duct with the circular groove is quite low and the fluid leaves the duct directly. Small clockwise vortex movements occur in the circular grooves. When baffles are added to the duct, the fluid can be directed to the grooves. Although this orientation increases with the increase of the baffle angle, it becomes especially evident with the increase in the baffle height which intensifies vortex formation in the grooves. While jet flow-like flow characteristics occur along the duct at  $60^\circ$  and  $90^\circ$  baffle angles at  $0.75H$  baffle height, the most movement of fluid in circular grooved ducts is obtained at a baffle angle of  $90^\circ$  and height of  $0.75H$  where the vortex motion in the circular grooves reaches a maximum level.
- The temperature of the fluid entering the grooved ducts increases according to the amount of contact with the hot grooves thanks to the baffles and the degree of turbulence created in the duct. However, increasing the baffle's angle and height allows the fluid to be better directed into the circular grooves. Fluctuations in temperature seen from the  $Z^* = 0.1-0.4$  parts of the ducts starting from the  $0.25H-60^\circ$  to  $0.75H-90^\circ$  baffled duct are due to the movement of the fluid impinging the first row of baffle in the duct after the first circular groove. While the highest temperature fluctuation seen in this part of the duct is in the baffled duct with  $0.5H-90^\circ$ , these changes in temperature compared to the non-baffle duct are a result of the enhancement in the heat transfer.
- With the rise in the Re number, the  $Nu_m$  number also enhances depending on the heat transfer increase from the circular groove ducts. For all three baffle heights, while the number of  $Nu_m$  rises with the increase of the baffle angle compared to the without baffle situation, the highest  $Nu_m$  value is reached at  $90^\circ$  angle and  $0.75H$  height. For  $Re = 6000$ , the increase in the number of  $Nu_m$  is 180.48% in the duct with a  $90^\circ$  angle and  $0.75H$  baffle height compared to the duct without a baffle.
- As the increase in Re number will intensify the movements of the vortexes in the circular grooves of the duct, the amount of  $Q$  to the fluid also increases. For  $Re = 3000$ , an increase of 53.42% and 87.33% in  $Q$  value is obtained in ducts with a  $60^\circ$  angle and  $0.75H$  height of the baffle compared to ducts with  $0.5H$  and  $0.25H$  baffle height, respectively.
- In parallel with the rise in the Re number, the turbulence intensity in the baffle tips and between them and also in the circular grooves rises with the rise in the angle and height of the baffle in the duct. For  $Re = 6000$ , the mean TKE value in a duct with a  $90^\circ$  baffle angle and  $0.25H$  height is %97.12 higher than in the duct without a baffle. This value increases to higher values when the baffle height is increased.
- In the duct with  $0.5H$  baffle height and  $90^\circ$  angle, and Re number of 6000, the increase in TKE value is 393.8% compared to the non-baffle duct.



**Fig. 13** Pressure variations along the upper midpoints parts of circular grooved rectangular ducts non-baffle, and with baffle angles of 30°, 60°, and 90°, and baffle heights of 0.25H, 0.5H, and 0.75H for distinct Re numbers

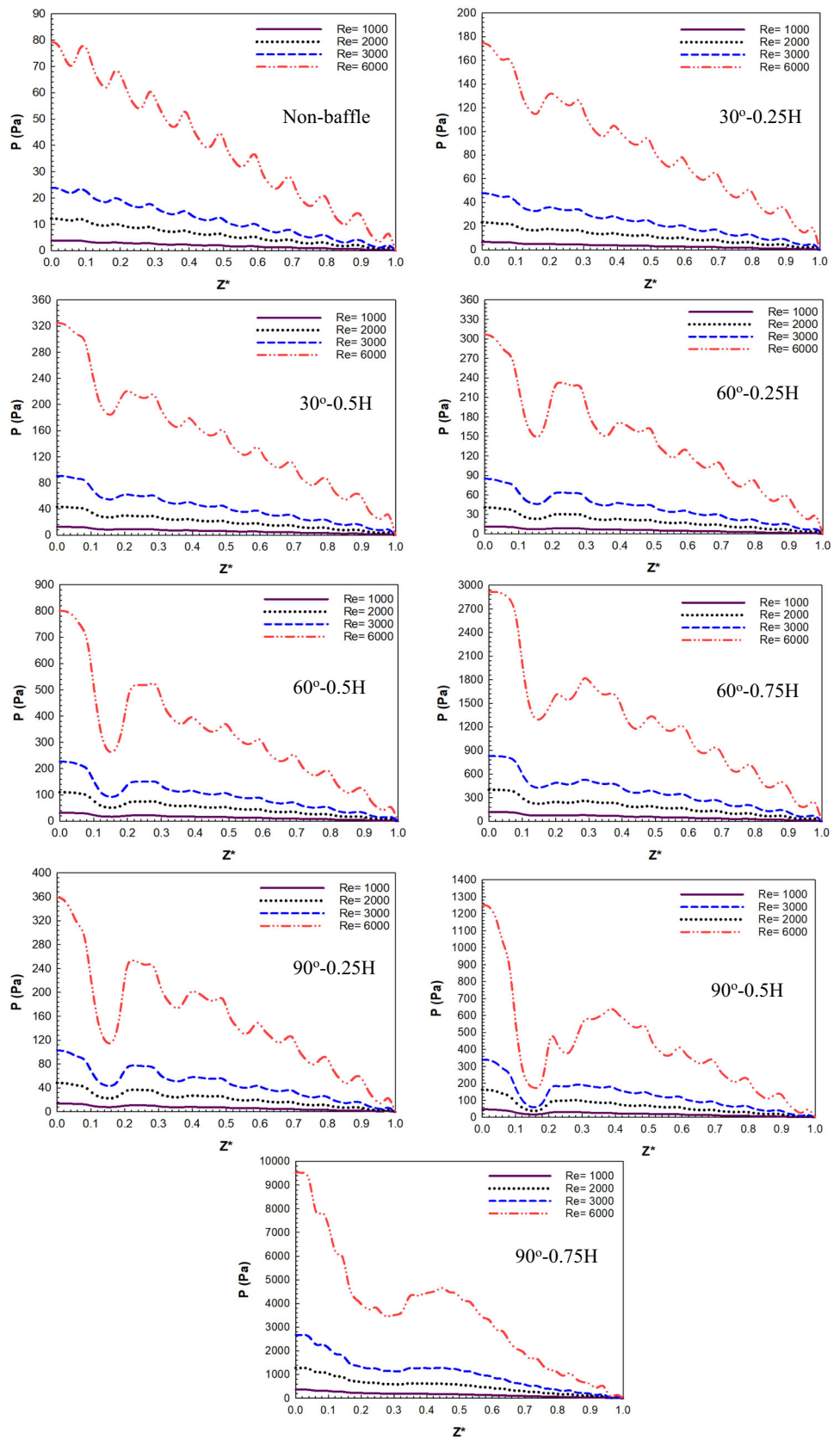
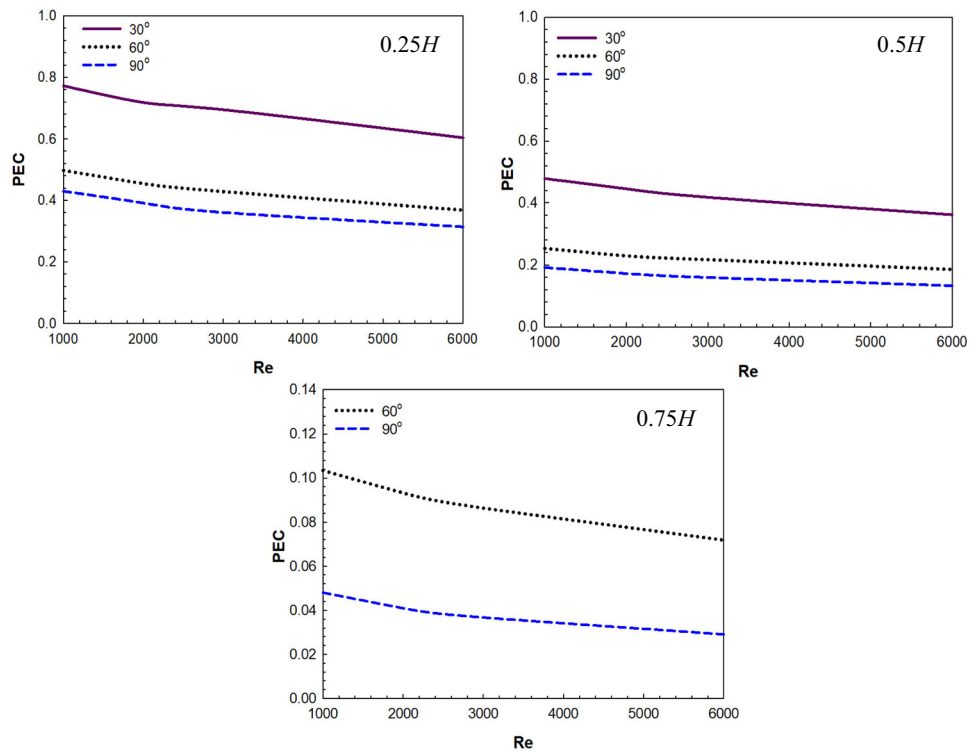


**Fig. 14** PEC number variations of circular grooved rectangular ducts non-baffle, and with baffle angles of 30°, 60°, and 90° for the baffle heights of 0.25*H*, 0.5*H*, and 0.75*H*



- When the baffle angle value is reduced from 90° to 30° at a baffle height of 0.25*H* for the  $Re = 6000$ , the increase in value of the TKE decreases to 24.64%. This proves that the baffle height is more decisive on the increase in TKE.
- Due to the fact that the baffle prevents the flow by decreasing the cross-sectional area of flow at the inlet of the duct, higher pressure values are obtained at the inlet in baffled ducts than in the non-baffled duct. However, while the pressure values decrease from the entrance to the exit of the circular grooved ducts, they increase with the increase in the  $Re$  number. The highest  $\Delta p$  is attained in the circular grooved duct with an angle of baffle of 90° and 0.75*H* height considering all baffle arrangements. Besides, there are fluctuations in the pressure values in the ducts depending on the baffle angle and height. The difference of pressure between the duct entry and exit is obtained with 9534 Pa for  $Re = 6000$  and 90° angle and 0.75*H* baffle height.
- As the baffle angle and height increase, the PEC number values decrease because the drop of pressure in the ducts increases. The rise in the  $Re$  number also causes a decrease in PEC values as it increases the  $\Delta p$ . However, since the rise in the value of the  $Nu$  number is higher against the  $\Delta p$ , it is determined that the best value of PEC is reached in the circular grooved duct with an angle of baffle of 30° and a height of 0.25*H*. For  $Re = 6000$  and 30° baffle angle, the PEC value at 0.25*H* baffle height is 66.88% higher than that in the 0.5*H*. These increment values reach much higher levels when compared to a 90° angle and a baffle height of 0.75*H*.
- While increasing the baffle angle and height increases the  $Nu_m$  number, they reduce the thermal–hydraulic performances of the grooved ducts. Thus, it is necessary to consider the number of PEC to make a full assessment of baffle arrangement effectiveness.
- In addition, the effect of reducing the baffle height is greater than the decrease in the baffle angle on the rise of the PEC number.

As a result, the addition of baffles with different angle and height arrangements to the circular grooved ducts provides an important increase in heat transfer while causing a negligible pressure drop. For this reason, it is thought that the outcomes of this work will benefit engineers working in the application of grooved heat exchangers, which have been intensively studied in recent years.

However, no results have been obtained because the 30° angled baffle at the end of the channel protruded from the channel at 0.75*H* baffle height. Besides this, it is aimed to improve the usability of the models in the study by using nanofluids whose thermophysical properties will be obtained experimentally in future works and to widely use the channel applications in the industry.

**Funding** Open access funding provided by the Scientific and Technological Research Council of Türkiye (TÜBİTAK).

**Data availability statement** The data that support the findings of this study are available from the corresponding author upon reasonable request.

## Declarations

**Conflict of interest** The authors declare that they have no known competing financial interests or personal relationships that could have appeared to influence the work reported in this paper. The authors declare the following financial interests/personal relationships which may be considered as potential conflict of interest.

**Open Access** This article is licensed under a Creative Commons Attribution 4.0 International License, which permits use, sharing, adaptation, distribution and reproduction in any medium or format, as long as you give appropriate credit to the original author(s) and the source, provide a link to the Creative Commons licence, and indicate if changes were made. The images or other third party material in this article are included in the article's Creative Commons licence, unless indicated otherwise in a credit line to the material. If material is not included in the article's Creative Commons licence and your intended use is not permitted by statutory regulation or exceeds the permitted use, you will need to obtain permission directly from the copyright holder. To view a copy of this licence, visit <http://creativecommons.org/licenses/by/4.0/>.

## References

- K. Karabulut, Heat transfer and pressure drop evaluation of different triangular baffle placement angles in cross-corrugated triangular channels. *Therm. Sci.* **24**(1), 355–365 (2020). <https://doi.org/10.2298/TSCI190813466K>
- C.N. Feng, C.H. Liang, Z.X. Li, Friction factor and heat transfer evaluation of cross-corrugated triangular flow channels with trapezoidal baffles. *Energy Build.* **257**, 111816 (2022). <https://doi.org/10.1016/j.enbuild.2021.111816>
- X.P. Liu, J.L. Niu, Effects of geometrical parameters on the thermohydraulic characteristics of periodic cross-corrugated channels. *Int. J. Heat Mass Transf.* **84**, 542–549 (2015). <https://doi.org/10.1016/j.ijheatmasstransfer.2015.01.046>
- Z. Chen, D. Zhao, T. Jiang, W. Xu, L. Jiang, X. Liu, G. Guan, Design and optimization of cross-corrugated triangular ducts towards reducing CO<sub>2</sub> emission and improving energy efficiency. *Aerosol Air Qual. Res.* **21**(12), 210184 (2021). <https://doi.org/10.4209/aaqr.210184>
- Z. Chen, Laminar forced flow and heat transfer in cross-corrugated triangular ducts. *Heat Trans. Eng.* **37**(16), 1392–1400 (2016). <https://doi.org/10.1080/01457632.2015.1136153>
- Y. Men, C. Liang, Z. Li, X. Tong, Configuration optimization of a membrane-based total heat exchanger with cross-corrugated triangular ducts considering thermal economy and entropy generation. *Case Stud. Therm. Eng.* **28**, 101446 (2021). <https://doi.org/10.1016/j.csite.2021.101446>
- A. Sharif, B. Ameel, I.T. Jollyn, S. Lecompte, M.D. Paeppe, Comparative performance assessment of plate heat exchangers with triangular corrugation. *Appl. Therm. Eng.* **141**, 186–199 (2018). <https://doi.org/10.1016/j.applthermaleng.2018.05.111>
- W.W. Focke, P.G. Knibbe, Flow visualization in parallel-plate ducts with corrugated walls. *J. Fluid Mech.* **165**, 73–77 (1986). <https://doi.org/10.1017/S0022112086003002>
- D. Hall, K. Scott, R.J.J. Jachuck, Determination of mass transfer coefficient of a cross-corrugated membrane reactor by the limiting-current technique. *Int. J. Heat Mass Transf.* **44**(12), 2201–2207 (2001). [https://doi.org/10.1016/S0017-9310\(00\)00274-X](https://doi.org/10.1016/S0017-9310(00)00274-X)
- L. Zhang, D.F. Che, Influence of corrugation profile on the thermal-hydraulic performance of cross-corrugated plates. *Numer. Heat Trans. Part A: Appl.* **59**(4), 267–296 (2011). <https://doi.org/10.1080/10407782.2011.540963>
- C.W. Leung, S.D. Probert, Forced convection turbulent flows through horizontal ducts with isosceles-triangular internal cross-sections. *Appl. Energy* **57**(1), 13–24 (1997). [https://doi.org/10.1016/S0306-2619\(96\)00021-9](https://doi.org/10.1016/S0306-2619(96)00021-9)
- L.Z. Zhang, Numerical study of periodically fully developed flow and heat transfer in cross-corrugated triangular channels in transitional flow regime. *Numer. Heat Trans. Part A: Appl.* **48**(4), 387–405 (2005). <https://doi.org/10.1080/10407780590957314>
- J.H. Doo, M.Y. Ha, J.K. Min, R. Stieger, A. Rolt, C. Son, An investigation of cross corrugated heat exchanger primary surfaces for advanced inter-cooled-cycle aero engines (Part-I: Novel geometry of primary surface). *Int. J. Heat Mass Transf.* **55**(19–20), 5256–5267 (2012). <https://doi.org/10.1016/j.ijheatmasstransfer.2013.01.084>
- H.H.S. Villanueva, P.E.B. Mello, Heat transfer and pressure drop correlations for finned plate ceramic heat exchangers. *Energy* **88**, 118–125 (2015)
- K. Nilpueng, S. Wongwises, Experimental study of single-phase heat transfer and pressure drop inside a plate heat exchanger with a rough surface. *Exp. Therm. Fluid Sci.* **68**, 268–275 (2015). <https://doi.org/10.1016/j.energy.2015.04.017>
- Y.F. Zhang, C. Jiang, Z. Yang, Y. Zhang, B. Bai, Numerical study on heat transfer enhancement in capsule-type plate heat exchangers. *Appl. Therm. Eng.* **108**, 1237–1242 (2016). <https://doi.org/10.1016/j.applthermaleng.2016.08.033>
- J. Wajs, D. Mikielwicz, Influence of metallic porous microlayer on pressure drop and heat transfer of stainless steel plate heat exchanger. *Appl. Therm. Eng.* **93**, 1337–1346 (2016). <https://doi.org/10.1016/j.applthermaleng.2015.08.101>
- K. Nilpueng, T. Keawkamrop, H.S. Ahn, S. Wongwises, Effect of chevron angle and surface roughness on thermal performance of single-phase water flow inside a plate heat exchanger. *Int. Commun. Heat Mass Trans. Commun. Heat Mass Trans.* **91**, 201–209 (2018). <https://doi.org/10.1016/j.icheatmasstransfer.2017.12.009>
- Z.X. Li, Y.Y. Gao, Numerical study of turbulent flow and heat transfer in cross-corrugated triangular ducts with delta-shaped baffles. *Int. J. Heat Mass Transf.* **108**, 658–670 (2017). <https://doi.org/10.1016/j.ijheatmasstransfer.2016.12.054>
- Z.S. Li, S.Q. Sun, C. Wang, C.H. Liang, S. Zeng, T. Zhong, W.P. Hu, C.N. Feng, The effect of trapezoidal baffles on heat and flow characteristics of a cross-corrugated triangular duct. *Case Stud. Therm. Eng.* **33**, 101903 (2022). <https://doi.org/10.1016/j.csite.2022.101903>
- C.H. Liang, C.N. Feng, T.Y. Lei, Z.X. Li, Numerical studies on the effect of baffle on the heat transfer and flow in cross-corrugated triangular ducts. *IOP Conf. Series: Earth Environ. Sci.* **238**(1), 0120286 (2019). <https://doi.org/10.1088/1755-1315/238/1/012086>
- FLUENT User's Guide, Fluent Inc. (Lebanon, Netherland, 2003), pp. 6–31.
- K. Karabulut, D.E. Alnak, Study of cooling of the varied designed warmed surfaces with an air jet impingement. *Pamukkale Univ. J. Eng. Sci.* **26**(1), 88–98 (2020). <https://doi.org/10.5505/pajes.2019.58812>
- K. Karabulut, Heat transfer improvement study of electronic component surfaces using air jet impingement. *J. Comput. Electron. Comput. Electron.* **18**, 1259–1271 (2019). <https://doi.org/10.1007/s10825-019-01387-3>
- J. Welty, G.L. Rorrer, D.G. Foster, *Fundamentals of Momentum, Heat, and Mass Transfer*, 6th edn. (Wiley, United States, 2014), p.298
- M. Akbarzadeh, S. Rashidi, J.A. Esfahani, Influences of corrugation profiles on entropy generation, heat transfer, pressure drop, and performance in a wavy channel. *Appl. Therm. Eng.* **1**, 278–291 (2017). <https://doi.org/10.1016/j.applthermaleng.2017.01.076>
- K. Scott, J. Lobato, Mass transport in cross-corrugated membranes and influence of TiO<sub>2</sub> for separation processes. *Indust. Eng. Chem. Res.* **42**(22), 5697–5701 (2003). <https://doi.org/10.1021/ie030374b>

28. L.Z. Zhang, Convective mass transport in cross-corrugated membrane exchangers. *J. Membr. Sci. Membr. Sci.* **260**, 75–83 (2005). <https://doi.org/10.1016/j.memsci.2005.03.029>
29. R.K. Ajeel, W.S.-I.W. Salim, K. Sopian, M.Z. Yusoff, K. Hasnan, A. Ibrahim, A.H.A. Al-Walei, Turbulent convective heat transfer of silica oxide nanofluid through corrugated channels: an experimental and numerical study. *Int. J. Heat Mass Transf.* **145**, 1–15 (2019). <https://doi.org/10.1016/j.ijheatmasstransfer.2019.118806>
30. R.K. Ajeel, W.S.-I.W. Salim, K. Hasnan, An experimental investigation of thermal-hydraulic performance of silica nanofluid in corrugated channels. *Adv. Powder Technol.* **30**(10), 2262–2275 (2019). <https://doi.org/10.1016/j.appt.2019.07.006>